Journal of Microscopy, Vol. 224, Pt 2 November 2006, pp. 158–165
Received 17 November 2005; accepted 12 May 2006

Mosaicing of microscope images with global geometric and radiometric corrections

CHANGMING SUN*, RICHARD BEARE*[1],
VOLKER HILSENSTEIN† & PAUL JACKWAY†
*CSIRO Mathematical and Information Sciences, Locked Bag 17, North Ryde, NSW 1670, Australia
†CSIRO Mathematical and Information Sciences, 306 Carmody Road, St Lucia, QLD 4067, Australia

Key words. Feature matching, global geometric correction, global radiometric correction, mosaicing, virtual microscope.

Summary

Image mosaicing has found a number of applications such as panoramic imaging, digital terrain mapping, ophthalmology and virtual microscopy. In this study, we present an automated mosaicing technique for generating virtual slides from microscope images. We carried out robust image feature matching and global geometric and radiometric parameter estimation. The input images were transformed using the estimated geometric and radiometric parameters and mosaiced together, producing accurate registration of overlapping regions without visible seams.

Introduction

Image mosaicing, also known as image montaging, image stitching or image tiling, has a wide range of applications such as panoramic image generation from several individual photographs (Capel & Zisserman, 1998; Shum & Szeliski, 2000; Isgro & Pilu, 2004), digital terrain generation for a large area (Wu & Campbell, 2004), mosaicing of fundus angiograms under ophthalmoscopes (Becker *et al.*, 1998; Zhou *et al.*, 2003) and slide generation for a virtual microscope that can be used locally or remotely over the internet.

A virtual slide system that employs a combination of enhanced software, image capture and processing techniques designed for telepathology was presented by Leong & McGee (2001). Possible applications of virtual microscopy are in diagnostic cytopathology (Steinberg & Ali, 2001), pathology (Molnar *et al.*, 2003; Saeger *et al.*, 2003) and teaching (Harris *et al.*, 2001; Blake *et al.*, 2003). The concept of virtual slides has also been called virtual case (Demichelis *et al.*, 2002). Ott (1997) reported an algorithm and its implementation in public domain software that works with an unmodified microscope without a motorized stage. Romer *et al.* (2003) reported the use of a modified standard microscope to generate virtual slides.

A manual method for seamlessly mosaicing confocal microscope images for visualization of neural networks was presented in Beck *et al.* (2000). Dani & Chaudhuri (1995) proposed techniques for automated mosaicing of retinal and satellite images using correlation and pyramidal approaches. The reference image was chosen arbitrarily first and the remaining images were processed sequentially. Bradley *et al.* (2005) described a virtual microscope system based on JPEG 2000. They used an extended depth of field to improve image quality. The mosaicing approach that they used is sequential. Appleton *et al.* (2005) presented an image mosaicing method based on dynamic programming for a row of images of a larger set. Duffin & Barrett (1998) presented an optimal solution for the most general case of geometric transformations. However, they did not carry out radiometric correction. There are also a number of commercial microscope systems that produce virtual slides that can handle large image overlaps (Bacus Laboratories, Inc., 2006; Soft Imaging System GmbH, 2006).

The mosaicing solutions mentioned above involve manual intervention or use a sequential approach for parameter estimation and are therefore not optimal. The optimal solution given in Duffin & Barrett (1998) used general transformation parameters for the images and did not carry out radiometric correction. In this work, we focus on a solution for creating an image mosaic from a microscope where images are obtained with an automated XY stage and the area of overlap can be as low as 5%. The number of parameters to be estimated for microscope images is much smaller than that of general computer vision applications due to the motion constraints of the XY stage.

Correspondence to: Dr Changming Sun. Tel: +61 2 9325 3207; Fax: +61 2 9325 3200; e-mail: changming.sun@csiro.au
[1]Present address: Medicine, Nursing and Health Sciences, Monash University, Melbourne, Victoria 3800, Australia.

Table 1. The features of the two cameras used for capturing the sample images.

	MicroPublisher 3.3 RTV	Evolution QEi
Sensor type	Colour CCD (Bayer pattern)	Cooled CCD
CCD chip	Sony ICX252AQ	Sony ICX285
Pixel size (μm)	3.45 × 3.45	6.45 × 6.45
Image size (pixels)	2048 × 1536	1392 × 1040

CCD, charge-coupled device.

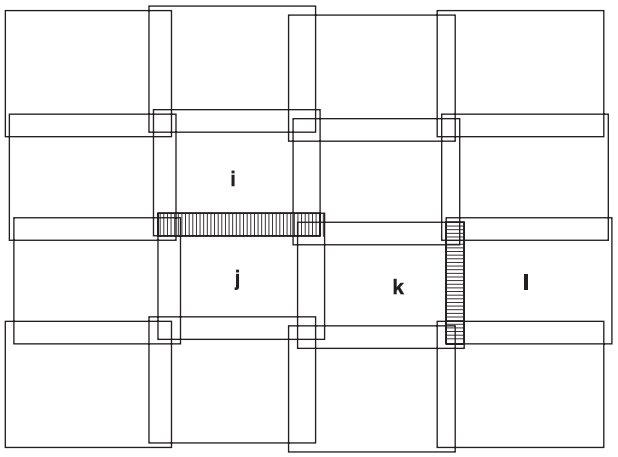

Fig. 1. Illustration of image overlaps between neighbouring image pairs. Two shaded overlap regions are shown in this figure: the vertical overlap between images 'i' and 'j', and the horizontal overlap between images 'k' and 'l'.

In this study, we propose algorithms for automatically estimating globally optimal geometric and radiometric transformation parameters for mosaicing microscope images. Geometric transformation is used to correct geometric inconsistency among all of the images and the radiometric transformation is used to balance variations in intensity due to inhomogeneous illumination within and across images. In a first optimization step, the geometric transformation parameters for all of the images are estimated simultaneously. A subsequent optimization step is used to estimate the radiometric transformation parameters for all images simultaneously.

Materials and methods

Image acquisition

The images presented here for our example applications were acquired using an Olympus BX61 microscope (Olympus, Tokyo, Japan) that was equipped with a motorized precision stage (model H101, Prior, Rockland, MA). The positioning accuracy of the stage is 3 μm. All images were acquired using a 20× Olympus UPlanFL objective lens.

Sample images for mosaicing were acquired using two different cameras. A Media Cybernetics Evolution QEi camera (Media Cybernetics, Silver Spring, MD) was used to capture images of fluorescently labelled bacteria and a QImaging (Burnaby, BC, Canada) MicroPublisher 3.3 RTV colour camera was used to capture images of histology sections. The relevant features of the two cameras are given in Table 1.

The spatial scale factor was estimated for both cameras in combination with the 20× lens. To determine this scale factor, the stage was moved over a known distance and the shift of a feature point in pixels was recorded. This produced initial estimates for the scale factors for the two cameras. These initial estimates were subsequently refined during the geometric parameter optimization process.

The automated stage allowed images to be captured at well-defined positions on a rectangular grid with approximately known overlap between neighbouring images. However, misalignment between the camera and the XY stage because of the camera X and Y axes not being parallel to the X and Y axes of the stage movement (hence the existence of a rotation angle between the camera X axis and the stage X axis), as well as mechanical inaccuracies, led to positioning errors such that features in overlapping images are not perfectly aligned as illustrated in Fig. 1.

Image feature detection and matching

Based on the position information of the microscope stage and the scale factor, approximate overlap regions between neighbouring images can be estimated as illustrated in Fig. 1 for the vertical overlap region between images 'i' and 'j' and the horizontal overlap region between images 'k' and 'l'. For each neighbouring image pair, the approximate overlap region can be calculated and used to constrain the search area for feature detection and matching.

We used the Harris corner detector to identify candidate feature points for matching (Harris & Stephens, 1988). The detected features in the two overlapping image patches were then matched using correlation and relaxation techniques as described in Zhang *et al.* (1995). Local consistency was used to further improve matching results (Kanazawa & Kanatani, 2004). The obtained feature matches were also used to fit a first-order warping function and matches with large residuals to the warping function were removed. An example match result is given in Fig. 2. The two images are a pair of overlapping image patches in neighbouring images. Figure 2(B) shows some matched feature points; the white dots indicate the feature location in one of the images and the black lines show the shift vectors for the corresponding points in the other image.

The shift vectors from all of the image pairs were used to estimate the geometric transformation parameters, whereas

Fig. 2. Example of overlap regions (A and B) of neighbouring images and some matched feature points shown as shift vectors (B).

intensity information from matched points was used to estimate the radiometric or intensity transformation parameters.

Global geometric transformation estimation

Parameters that are part of a general transformation model include translations in the X and Y directions, image rotation, camera zoom or scaling factor, camera pan and tilt angles, and lens distortion. The rotation is caused by misalignment of the camera sensor and stage axis as well as mechanical errors. For the present application in microscopy, we only considered two geometric parameters (the X and Y translations) for each image, one parameter for the image rotation angle (as the XY stage was used, the angle for each image should stay constant) and two parameters for the scaling factor along the X and Y axes for all of the images. We used the following objective function for estimating all of the geometric transformation parameters simultaneously

$$f_g(X_1, Y_1, \ldots, X_N, Y_N, \theta, s_x, s_y) = \sum_{p=1}^{P} \sum_{m=1}^{M_p} \left\| T^g(x_{im}, y_{im})|_{X_i, Y_i, \theta, s_x, s_y} - T^g(x_{jm}, y_{jm})|_{X_j, Y_j, \theta, s_x, s_y} \right\|^2 \quad (1)$$

where N is the number of images; i, j are image indices, $1 \leq \{i, j\} \leq N$; P is the number of overlap regions among which image matching is carried out and M_p is the number of matched features for overlap region p. (x_{im}, y_{im}) and (x_{jm}, y_{jm}) are a pair of matching points in images i and j, respectively. The match point positions (x_{im}, y_{im}) and (x_{jm}, y_{jm}) are in the original input image coordinate system, not in the local system of the overlapping image patches. The T^gs are the geometric transformations for each image. These involve translation, rotation and scaling. X_i, Y_i are the translation parameters to be estimated for image i. θ is the image rotation angle for all of the images. The parameters s_x, s_y are the scaling factors, which will be the same for all of the images. The total number of parameters is $2N + 3$. In the above objective function, we tried to minimize the Euclidean distance of matched feature point positions when the transformation parameters were applied. The resulting transformation parameters were used to align the images and thus construct the mosaic.

Global radiometric transformation estimation

Image mosaics constructed using the geometric transformations described above will typically have visible seams due to lighting variations within and across images. For seamless mosaics, one also needs to correct for the uneven lighting within an image and the intensity differences between neighbouring images. The latter could be due to asymmetrical background lighting and the overlapping regions being from different images and from different sides of the image centre. It would also arise from fluctuations in the brightness of the light source and, to some extent, differences in local thickness of the embedding medium. For colour images, we calculated the average intensity from all channels. Therefore, we had the same number of parameters for colour as for monochrome images.

Global radiometric correction was carried out using a similar approach to geometric correction – an objective function including intensity information from matched points was optimized. The objective function with all of the parameters, which will be estimated simultaneously, is

$$\begin{aligned} f_r(a_1, b_1, c_1, d_1, e_1, f_1, \ldots, a_N, b_N, c_N, d_N, e_N, f_N,) = & \sum_{p=1}^{P} \sum_{m=1}^{M_p} \left| I_i(x_{im}, y_{im}) T^r(x_{im}, y_{im})|_{a_i, b_i, c_i, d_i, e_i, f_i} \right. \\ & \left. - I_j(x_{jm}, y_{jm}) T^r(x_{jm}, y_{jm})|_{a_j, b_j, c_j, d_j, e_j, f_j} \right| \\ & + \sum_{i=1}^{N} \sum_{n=1}^{N_i} |I_i(x_{in}, y_{in}) T^r(x_{in}, y_{in})|_{a_i, b_i, c_i, d_i, e_i, f_i} - I_{\text{mean}}| \end{aligned} \quad (2)$$

The notation is similar to that used in Eq. (1). T^r is the radiometric transformation function for each image. a_i, b_i, c_i, d_i, e_i and f_i are the parameters to be estimated for image i. $I_i(x_{in}, y_{in})$ is the image intensity at position (x_{in}, y_{in}) in image i. I_{mean} is the average image intensity value for all of the image components.

The first term on the right-hand side of Eq. (2) accounts for the transformed intensity difference between two neighbouring images. The second term on the right-hand side of Eq. (2) is the difference between the intensity transformed image and the average image intensity value. (x_{in}, y_{in}) are additional regularly spaced sample points in image i, which are not part of the matching points. N_i is the number of sample points. The reason for introducing these additional sample points in images is

that the features found by the corner detector are not representative as they are mostly on image boundaries. Additional points make parameter estimation more robust.

The function T^r, used in Eq. (2), is defined as

$$T^r(x_{im},y_{im})|_{a_i,b_i,c_i,d_i,e_i,f_i} = a_i x_{im}^2 + b_i x_{im} y_{im} + c_i y_{im}^2 + d_i x_{im} + e_i y_{im} + f_i \quad (3)$$

Other orders of polynomials, e.g. only using terms involving b_i, d_i, e_i and f_i, for T^r can also be used.

The radiometrically corrected image is obtained using the following formula for each image

$$I_i^{corrected} = I_i T^r \quad (4)$$

As the field of view of the microscope camera is small, the vignetting effect that may exist should be small and it can be modelled by the quadratic function given in Eq. (3). The parameters given in Eq. (2) are those for every image; hence the total number of parameters for radiometric correction will be $6N$ for N images in the parameter estimation stage. Due to this relatively large parameter number, a larger number of sampling points from each image will be needed such that enough constraints are available and the optimization process gives sensible results. This will lead to a slower estimation process.

The following alternative methods can also be used. The same quadratic function can be used for all of the images. In this case, only six parameters are needed for all of the images. Because of the confining environment of a microscope, the change of lighting condition is not large. Therefore, the use of a smaller number of parameters also gives sensible results. Radiometric or image background correction can also be carried out by modelling the intensity function using a white object at a separate calibration stage for estimating the background function if the computational cost of radiometric correction is an issue for certain applications.

For histology sections it is generally preferable to use a background calibration image to perform the intensity correction. Typically some calibration images need to be captured for white-balancing and the additional effort required to perform the corrections is minimal.

For fluorescence applications, however, this is not trivial as specific calibration slides are needed with homogeneous fluorescence and this is not always available. Also, some fluorescence that is outside the field of view sometimes spills over into the image. These background effects are different for every image and cannot be corrected for by using a single calibration image. However, a quadratic model is not necessarily appropriate for these types of effects.

Image mosaicing

Once the global geometric and radiometric transformation parameters are obtained, the images can be radiometrically corrected and geometrically warped. The transformed images are then stitched together to form a larger mosaic image that can then be used as a virtual slide.

The steps for creating a mosaic from a set of input images are as follows.

1 Estimate initial approximate overlap for neighbouring images and obtain overlapping image patches from the original images in these regions.
2 Carry out feature detection and matching for each pair of overlapping patches. Store the position and intensity information for each pair of patches.
3 Optimize geometric transformation parameters for all of the images simultaneously using the positions of the obtained matching features.
4 Optimize radiometric transformation parameters for all of the images simultaneously using the intensity and positional information of the obtained matching features (for the first term on the right-hand side of Eq. 2). A regular sampling of image positions and the associated image intensity information are also needed (for the second term on the right-hand side of Eq. 2).
5 Transform images using radiometric parameters using Eq. (4) for intensity correction.
6 Transform images using geometric parameters for alignment.
7 Combine the transformed images by simply using one of the images on the overlapping regions.

Results and discussion

This section shows some of the image mosaicing results obtained using our algorithm. We tested the algorithm on a variety of microscope images, both brightfield and fluorescence.

Figure 3 shows a set of images of a histology section to be mosaiced. This is a challenging image set as the amount of overlap for neighbouring images is only about 5% along each axis. Figure 4(A) shows an image mosaic obtained by simply tiling the images according to the position information of the microscope stage without applying further geometric and radiometric corrections. The misregistration of some features and intensity seams at image boundaries can be seen. Figure 4(B) shows an image mosaic with geometric and radiometric corrections. In this mosaic the misregistration and intensity seams present in Fig. 4(A) are removed.

Figure 5 shows another grid of images to be mosaiced. These images are of fluorescently labelled bacteria and are particularly challenging due to the small number of distinct feature points in the images. Figure 6(A) gives an image mosaic without geometric and radiometric corrections. Again, misregistration and intensity seams at image boundaries are clearly visible. Figure 6(B) gives an image mosaic with geometric and radiometric corrections. In this image, the features are well registered and intensity seams are not visible.

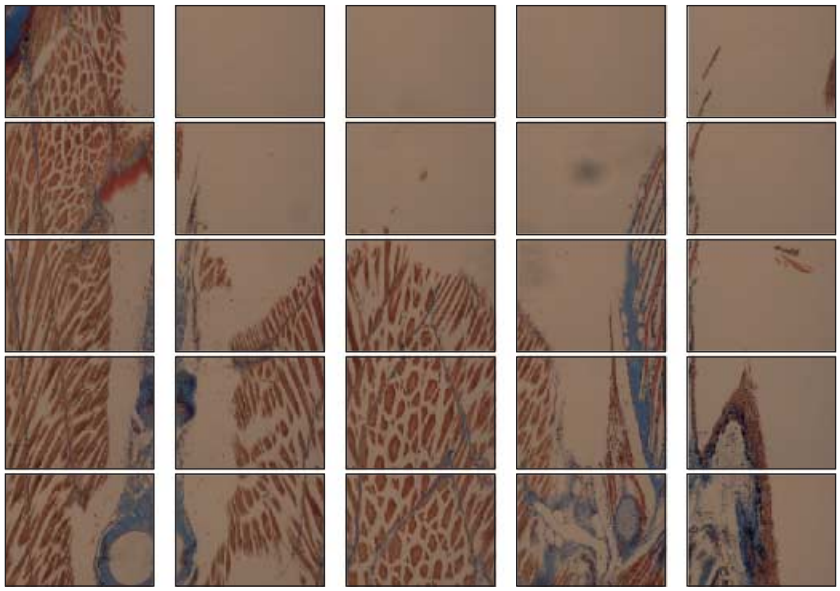

Fig. 3. Input 25 (5×5) histology images. The percentage of overlap is about 5%.

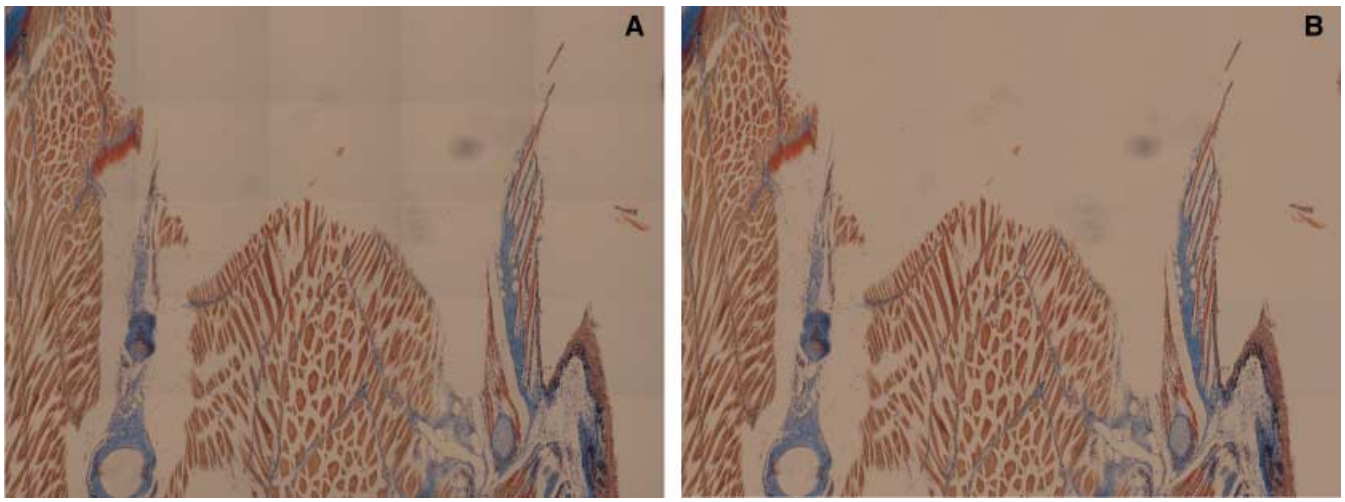

Fig. 4. Image mosaics without (A) and with (B) geometric and radiometric corrections.

Figure 7 shows a pair of subregions of mosaiced images of a different data set that contains 100 images, one without (Fig. 7A) and one with (Fig. 7B) the geometric and radiometric corrections. The large ellipses indicate the positions of horizontal boundaries, whereas the small ellipses give the vertical boundaries of neighbouring images. The arrows indicate the positions of image intensity differences for neighbouring images before and after radiometric correction. The good quality of mosaics obtained using our method is clearly visible.

Table 2 shows the times taken for each processing step for a set of 25 images on a computer with a 2.66-GHz Intel CPU. The parameter optimization was carried out using the Nelder-Mead method described in Nelder & Mead (1965).

Table 2. Timings for each processing step (for a set of 25 images).

	Timings (s)
Image feature detection and matching	3.19
Geometric parameter estimation	3.21
Radiometric parameter estimation	6.07
Image warping and mosaicing	11.39

To increase the speed of the mosaicing process, a smaller number of transformation parameters may be used. The optimization could also be carried out on a sequence of sub-blocks of images if the number of input images is very large.

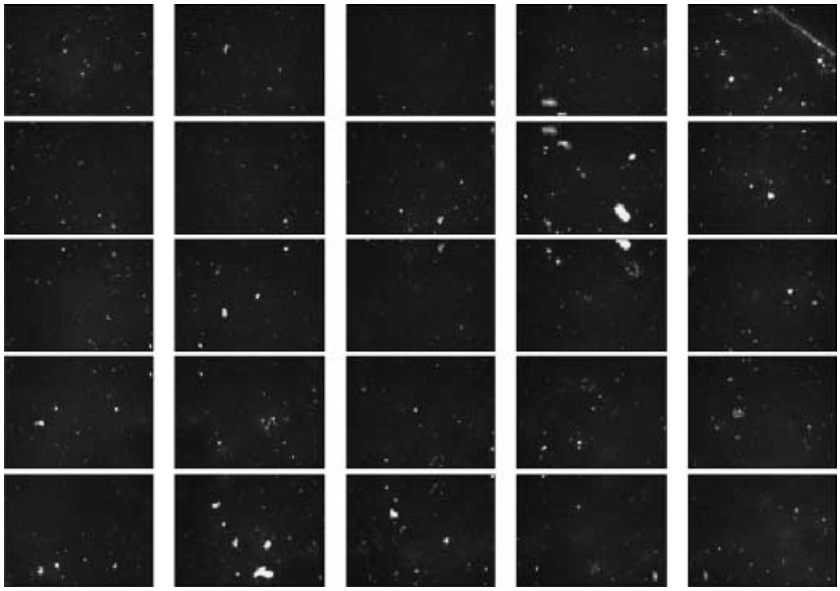

Fig. 5. Input 25 (5 × 5) images.

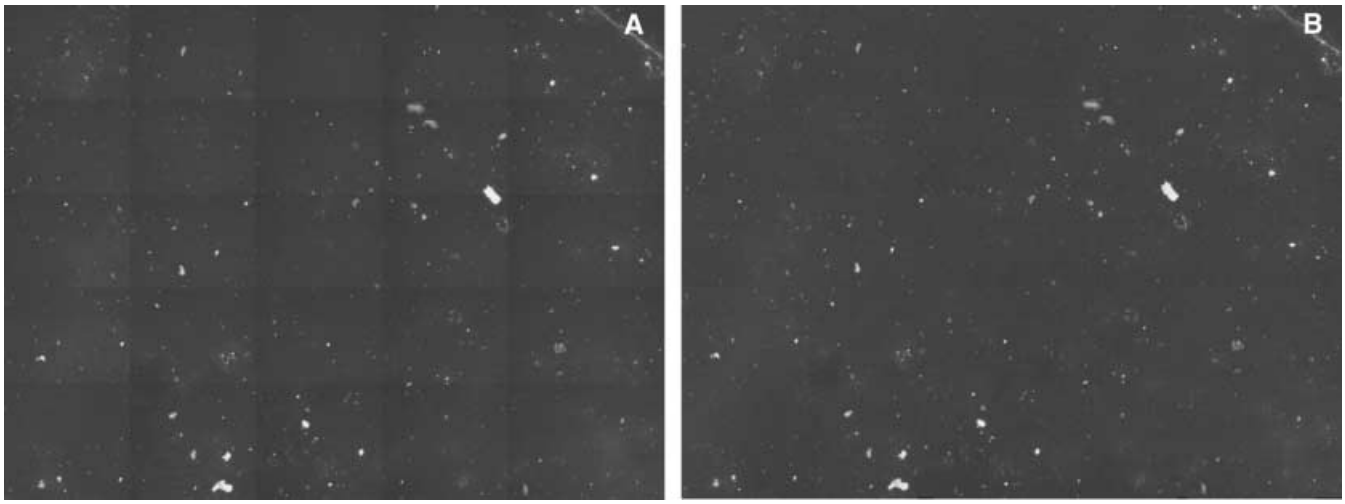

Fig. 6. Image mosaics without (A) and with (B) geometric and radiometric corrections.

As shown in the figures mentioned earlier, the use of global optimization for the geometric and radiometric parameters produces very good image mosaicing results. The global nature of the parameter optimization makes the best use of all of the available information. For most of the images in the input image grid, there are four overlap regions around each image (not counting the small overlap regions with diagonal neighbours). The image feature matching information around an image helps to stabilize the parameter estimation process. Local or partial optimization using a smaller number of images usually does not utilize all of the available information and hence the parameters estimated may not be optimal, especially when the image overlaps are small. The use of global optimization of all of the transformation parameters simultaneously can avoid the accumulation of small registration errors in approaches that start with one reference image and keep adding images.

Conclusions

Image mosaicing has found a number of applications. We have presented algorithms for the automatic estimation of globally optimal geometric transformation parameters for all of the images, and optimization of the radiometric correction parameters simultaneously for all of the images based on feature matching and image intensity information. The obtained parameters are then used for image warping, intensity correction and stitching. Results on real microscopy data

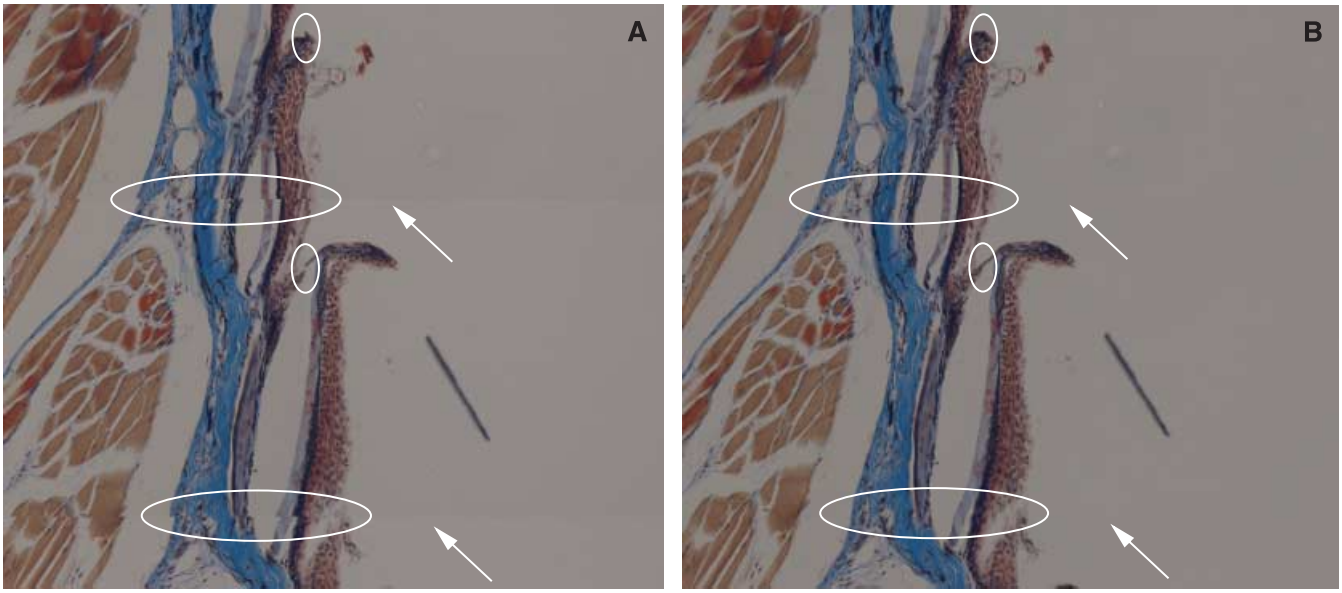

Fig. 7. Subregions of two large image mosaics without (A) and with (B) geometric and radiometric corrections.

sets show that our algorithm produces mosaics of high quality, with accurate registration and without visible intensity seams.

Acknowledgements

We thank the anonymous reviewers for their very constructive comments. The work was funded through the CSIRO P-Health Flagship program and we thank Dr Michael Conlon of CSIRO Human Nutrition for the preparation of the fluorescent slides. The preliminary conference version of this paper appeared in Sun *et al.* (2005).

References

Appleton, B., Bradley, A.P. & Wildermoth, M. (2005) Towards optimal image stitching for virtual microscopy. *Digital Image Computing: Techniques and Applications*, pp. 299–306. IEEE, Cairns, Australia.

Bacus Laboratories, Inc. (2006) http://www.bacuslabs.com/bliss.html

Beck, J., Murray, J., Willows, A. & Cooper, M. (2000) Computer-assisted visualizations of neural networks: expanding the field of view using seamless confocal montaging. *J. Neurosci. Meth.* **98** (2), 155–163.

Becker, D.E., Can, A., Turner, J.N., Tanenbaum, H.L. & Roysam, B. (1998) Image processing algorithms for retinal montage synthesis, mapping, and real-time location determination. *IEEE Trans. Biomed. Eng.* **45** (1), 105–118.

Blake, C.A., Lavoie, H.A. & Millette, C.F. (2003) Teaching medical histology at the University of South Carolina School of Medicine: Transition to virtual slides and virtual microscopes. *Anat. Rec. (Part B: New Anat.)*, **275** (1), 196–206.

Bradley, A.P., Wildermoth, M. & Mills, P. (2005) Virtual microscopy with extended depth of field. *Digital Image Computing: Techniques and Applications*, pp. 235–242. IEEE, Cairns, Australia.

Capel, D. & Zisserman, A. (1998) Automatic mosaicing with super-resolution zoom. *Proceedings of Computer Vision and Pattern Recognition*, pp. 885–891. IEEE, Washington, DC, U.S.A.

Dani, P. & Chaudhuri, S. (1995) Automated assembling of images: Image montage preparation. *Patt. Recog.* **28** (3), 431–445.

Demichelis, F., Barbareschi, M., Dalla Palma, P. & Forti, S. (2002) The virtual case: a new method to completely digitize cytological and histological slides. *Virchows Arch.* **441** (2), 159–164.

Duffin, K.L. & Barrett, W.A. (1998) Globally optimal image mosaics. *Graphics Interface*, pp. 217–222. Canadian Human-Computer Communications Society, Vancouver, BC, Canada.

Harris, C. & Stephens, M. (1988) A combined corner and edge detector. *Proceedings of the Fourth Alvey Vision Conference*, pp. 147–151. Alvey Vision Club, Manchester, U.K.

Harris, T., Leaven, T., Heidger, P., Kreiter, C., Duncan, J. & Dick, F. (2001) Comparison of a virtual microscope laboratory to a regular microscope laboratory for teaching histology. *Anat. Rec. (New Anat.)*, **265** (1), 10–14.

Isgro, F. & Pilu, M. (2004) A fast and robust image registration method based on an early consensus paradigm. *Patt. Recog. Lett.* **25** (8), 943–954.

Kanazawa, Y. & Kanatani, K. (2004) Robust image matching preserving global consistency. *Sixth Asian Conference on Computer Vision*, pp. 1128–1133. Asian Federation of Computer Vision Societies, Jeju Island, Korea.

Leong, F.J. & McGee, J.O. (2001) Automated complete slide digitization: a medium for simultaneous viewing by multiple pathologists. *J. Pathol.* **195** (4), 508–514.

Molnar, B., Berczi, L., Diczhazy, C., Tagscherer, A., Varga, S.V., Szende, B. & Tulassay, Z. (2003) Digital slide and virtual microscopy based routine and telepathology evaluation of routine gastrointestinal biopsy specimens. *J. Clin. Pathol.* **56** (6), 433–438.

Nelder, J.A. & Mead, R. (1965) A simplex algorithm for function minimization. *Comput. J.* **7** (4), 308–313.

Ott, S.R. (1997) Acquisition of high-resolution digital images in video microscopy: Automated image mosaicking on a desktop microcomputer. *Microsc. Res. Techn.* **38** (3), 335–339.

Romer, D.J., Yearsley, K.H. & Ayers, L.W. (2003) Using a modified standard microscope to generate virtual slides. *Anat. Rec. (Part B: New Anat.)*, **272** (1), 91–97.

Saeger, K., Schluns, K., Schrader, T. & Hufnagl, P. (2003) The virtual microscope for routine pathology based on a PACS system for 6 Gb images. *CARS 2003 – Computer Assisted Radiology and Surgery*, Vol. 1256, pp. 299–304. Elsevier Science; London QEII Conference Centre.

Shum, H.-Y. & Szeliski, R. (2000) Construction of panoramic image mosaics with global and local alignment. *Int. J. Comput. Vis.* **36** (2), 101–130.

Soft Imaging System GmbH (2006) http://www.softimaging.net/rd/english/3412.htm

Steinberg, D.M. & Ali, S.Z. (2001) Application of virtual microscopy in clinical cytopathology. *Diagn. Cytopathol.* **25** (6), 389–396.

Sun, C., Hilsenstein, V., Beare, R. & Jackway, P. (2005) Mosaicking of microscope images. *Digital Image Computing: Techniques and Applications*, pp. 343–348. IEEE, Cairns Convention Centre, Australia.

Wu, X. & Campbell, N.A. (2004) A colour-balancing method and its applications. *The 12th Australasian Remote Sensing and Photogrammetry Conference*, Fremantle, Spatial Science Institute, Western Australia.

Zhang, Z., Deriche, R., Faugeras, O. & Luong, Q.-T. (1995) A robust technique for matching two uncalibrated images through the recovery of the unknown epipolar geometry. *Artif. Intell.* **78** (1/2), 87–119.

Zhou, Y., Xue, H. & Wan, M. (2003) Inverse image alignment method for image mosaicing and video stabilization in fundus indocyanine green angiography under confocal scanning laser ophthalmoscope. *Comput. Med. Imag. Graph.* **27** (6), 513–523.

